Phase Synchronization in Neural Systems

Andreas Daffertshofer[1] and Bastian Pietras[2]
[1]Faculty of Behavioural and Movement Sciences, Amsterdam Movement Sciences & Institute for Brain and Behaviour Amsterdam, Vrije Universiteit Amsterdam, Amsterdam, The Netherlands
[2]Institute of Mathematics, Technische Universität Berlin and Bernstein Center for Computational Neuroscience Berlin, Berlin, Germany

Article Outline

Glossary

Neural spikes Discrete events as proxy for action potentials in single neurons.

Firing rate Population activity measured at each instant in time as the fraction of neurons that fire a spike within a certain time window.

Membrane potential Common state variable of a single neuron that induces a spike/an action potential once it has crossed a certain threshold.

Stable limit cycle A periodic orbit along which rhythmic activity emerges and that attracts all neighboring trajectories in its vicinity.

Neural oscillator A single neuron, a population of similar neurons, or a pair of excitatory and inhibitory neural populations that exhibit rhythmic activity.

Phase oscillator Reduced description of an oscillator with sole focus on the evolution of its phase.

Phase reduction Technique to identify the state of a (high-dimensional) oscillator through its phase on or in the immediate vicinity of the stable limit cycle.

Order parameters Common variables describing the (dis)order of a large system of many components.

Neural mass model Description of a neural population by means of its density, often parametrized by the mean and/or variance.

Definition of the Subject

Oscillatory neural activity is abound on all temporal and spatial scales. One can observe this on the microscopic level of neuronal circuits as well as on mesoscopic and macroscopic levels of neural populations. The latter give rise to brain rhythms that, dependent on their spectral properties, adhere to different function. A disruption of the interplay of this oscillatory activity is often deemed a signature of pathology (Schnitzler and Gross 2005; Uhlhaas and Singer 2006; Hutt and Buhry 2014). All the more it is important to understand the underlying mechanisms how these neural oscillations emerge and evolve and how oscillations of different populations interact and influence each other. Synchronous firing of individual neurons can give rise to large-scale oscillatory activity of a population, and the phase synchronization between populations is key for communication between them.

R. A. Meyers (ed.), *Encyclopedia of Complexity and Systems Science*,
https://doi.org/10.1007/978-3-642-27737-5_693-1

Introduction

The functioning of the brain dwells on coordinated and coherent coactivity of a multitude of neurons. Perceptual, cognitive, and motor functions are believed to require an orchestration of distributed neuronal processes. If spike discharges of a large number of neurons exhibit correlated behavior in different areas of the brain, their (large-scale) integration allows for sensory integration, the generation of motor commands, and cognitive processing. Unraveling these integration processes poses a challenge in itself and is often referred to as the *binding problem* (Singer 2007). Binding by convergence results in the grouping of specialized neurons that encode a particular fixed constellation of contextual features. Dynamic binding, by contrast, assembles individual neurons dynamically to generate and represent particular patterns at particular points in time (Nunez 2000). A neuron can participate in the representation of one pattern in one moment, but an instant later, it is involved in encoding another one. Synchronization of neuronal discharges at millisecond scale can yield sequences of subsequently active assemblies, which can effectively encode complex information to be exchanged among neuronal networks. And, this temporal organization of neuronal activity capitalizes on self-organized information retention and local-global integration. The ability to preserve and store information is equally important as integrating distributed local processes into globally ordered states and controlling local computations through global brain activity. Both are likely maintained by a hierarchy of brain rhythms (Buzsaki 2006). The temporal coordination of distributed brain activity, hence, strongly – if not solely – relies on the synchronization of neural oscillations (Gray 1994; MacKay 1997).

On macroscopic scales, brain rhythms and oscillatory population activity are the dominant observables. There are numerous approaches to unravel the orchestration of intertwined neural processes, both experimental and theoretical. Bridging the gap between experiments and theory, however, has only been achieved in very restrictive cases and mainly on very small spatial and temporal scales. An overall and generic picture linking these two sides of the same coin is still being sought for. Neuroimaging techniques such as magneto- and electroencephalography (M/EEG) reflect voltage fluctuations resulting from ionic currents in the neurons. Given the noninvasive nature of these techniques, the recorded data display synchronous activity of several thousands of interacting neurons rather than the dynamics of a single neuron. The population dynamics, or mean field behavior, has often very little in common with what happens on the microscopic scale.

An urgent challenge in theoretical neuroscience is to deduce macroscopic dynamics from activity on these much smaller scales (Haken 2006; Deco et al. 2008; Coombes 2010; Siettos and Starke 2016; Breakspear 2017). Yet, the plenitude of findings provide valuable guidelines for our understanding of neural synchronization processes on both micro- and macroscopic scales; see Fig. 1 for an example.

Micro- and Macroscopic Views

When characterized as rhythmic changes in, e.g., local field potentials, neural oscillations set a recurrent temporal reference frame. The ups and downs in fluctuating local field potentials reflect high and low degrees of synchronization of neuronal currents within a certain brain area. That is why synchronization and neural oscillations are often used interchangeably to express coherent activity of a population of neurons. However, there is a subtle difference between the two phenomena (Singer 1993). Oscillatory activity can be induced on a population level through single oscillatory neurons, so-called pacemaker cells. It may also manifest as an emergent property of the underlying network architecture when a particular dynamic circuit motif is activated. Such a motif comprises the physical circuit structure, its electrophysiological signature, and the corresponding computational function (Womelsdorf et al. 2014). Synchronization, on the other hand, can also occur in the absence of oscillations. Two cells may always discharge simultaneously but at

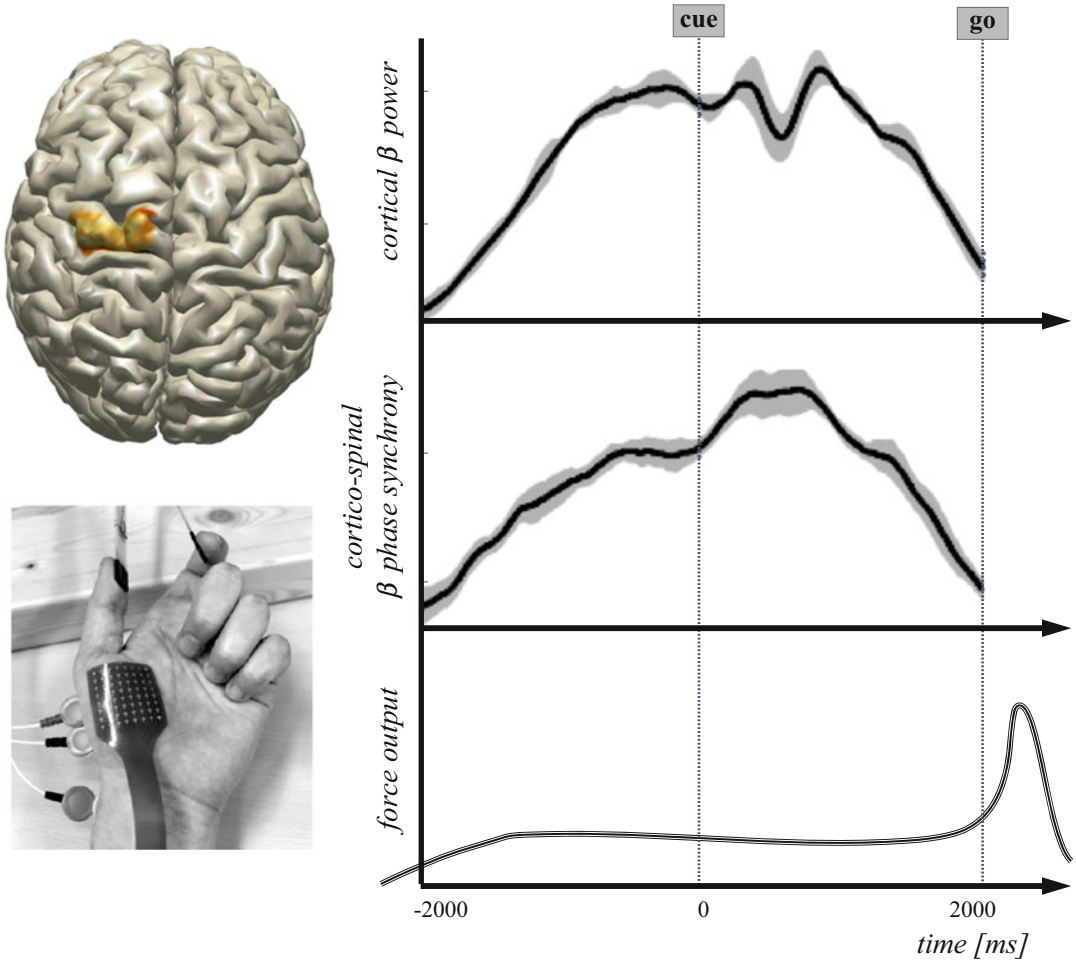

Phase Synchronization in Neural Systems, Fig. 1 Beta-range oscillatory activity measured via EEG over (here left) motor cortex and beta synchrony between cortex and spinal cord are up- or downregulated in anticipation of movement initiation. The temporal changes in local synchronization in motor cortex (top right panel: spectral power around 15–30 Hz) reflect a precision grip being produced with the right hand that ought to be changed after receiving a go-signal (lower right panel: force level). The corticospinal synchronization (middle right panel: phase synchronization between EEG-electromyographic signals of finger and thumb flexors) also follows that pattern although pre-cueing (cue-signal) 2 s ahead of movement initiation is seemingly not propagated along the corticospinal tract; see Van Wijk et al. (2008) for more details.

irregular intervals when driven by common noise. Or, a presented stimulus induces simultaneous bursting of neural populations. This is a typical signature of response synchronization. Synchronization may lead to oscillations, and oscillations may facilitate synchronization, but, in general, they are "just" indicative for synchrony.

While oscillatory population activity can be related to synchronous interactions of individual cells – we provide an example below – one must be careful when relating single cell responses to synchronous network activity. There is a micro-macro dichotomy with respect to the transition from individual neuronal dynamics to the collective behavior of a neural population. It may happen that individual discharges of a neuron are perfectly time-locked with the oscillating field potential while, e.g., the lagged autocorrelation of the discharges does not show any sign of oscillatory activity. The seminal work by Brunel and

Hakim offered a theoretical account of a collection of experimental studies hinting at sparse synchronization of neuronal networks (Brunel and Hakim 1999). By contrast, regular spiking activity of single neurons does not necessarily result in (regular) oscillations on the population level but may yield collective chaos (Pazó and Montbrió 2016). Likewise, asynchronous network states may emerge despite a considerable amount of shared input (Renart et al. 2010).

Correlated Behavior and Phase Synchronization

Discernible neural population activity depends on correlated activity of a large number of neurons (Wang 2010). When considering time series of experimental or synthetic data, synchronization can be identified through a variety of measures. They range from correlation coefficients to coherence, from phase coherence to Granger causality, from phase locking values to Kullback-Leibler information divergence, and from state space-based measures to stochastic event synchrony (Dauwels et al. 2010). Some of these measures show a strong correlation among one another, whereas others do not, but all of them have in common that they seek to quantify the degree to which firing rates of neurons are related (Golomb 2007).

When it comes to neural oscillations, focus is on the oscillations' amplitudes and frequencies. For a given frequency, one can define the period as the duration of time of one cycle of oscillation. In between a cycle, one can further define the *phase* of oscillation, which continuously increases between 0 and 2π. Phase and amplitude thus become the main (time-resolved) determinants of the state of oscillation. Phase synchronization measures aim at quantifying the closeness of the phases when mapped on the unit circle (Jean-Philippe et al. 1999). Phase synchronization measures are particularly suited for cases in which oscillatory units are weakly coupled because in that case dynamically changing amplitudes can be largely ignored. In the following, we concentrate on such cases. As we will show, phase synchronization is paramount for functional connectivity of the brain and communication between neural populations in general (Varela et al. 2001; Sauseng and Klimesch 2008; Thut et al. 2012).

From Single Cell Dynamics to Neural Masses: Synchronization in a Neural Population

A plethora of modeling approaches exists to link single cell dynamics to the dynamics of neural populations. Modeling boomed in the 1970s. It was Walter Freeman who introduced the notion of neural mass models, which are in essence descriptions of the dynamics of neural population densities (Deco et al. 2008; Freeman 1975). Many of these models are arguably heuristic in nature (Lopes da Silva et al. 1974; Amari 1977; Jansen and Rit 1995) and/or involve debatable approximations. Here we illustrate a proper deduction of population or neural mass dynamics starting at a well-defined single cell level.

We follow a recent study by Montbrió et al. (2015) and consider a large population of identical quadratic integrate-and-fire (QIF) neurons with the ultimate goal to derive the dynamics of the population's mean membrane potential V. The neurons are coupled with each other electrically via gap junctions of strength G and/or through chemical synapses of strength J with activation function S, as detailed below. We denote the individual membrane potentials by v_j with $j = 1,\ldots, N \gg 1$ and assume that they follow the dynamics

$$\tau \dot{v}_j = v_j^2 + n_j + G\big(V - v_j\big) + J\tau S, \qquad (1a)$$

where τ represents the membranes' time constant and η_j is an external input current flowing into neuron j. To model action potentials, or spikes, as sketched in Fig. 2 (upper panel), the continuous dynamics (1a) is accompanied by the following discrete fire and reset rule:

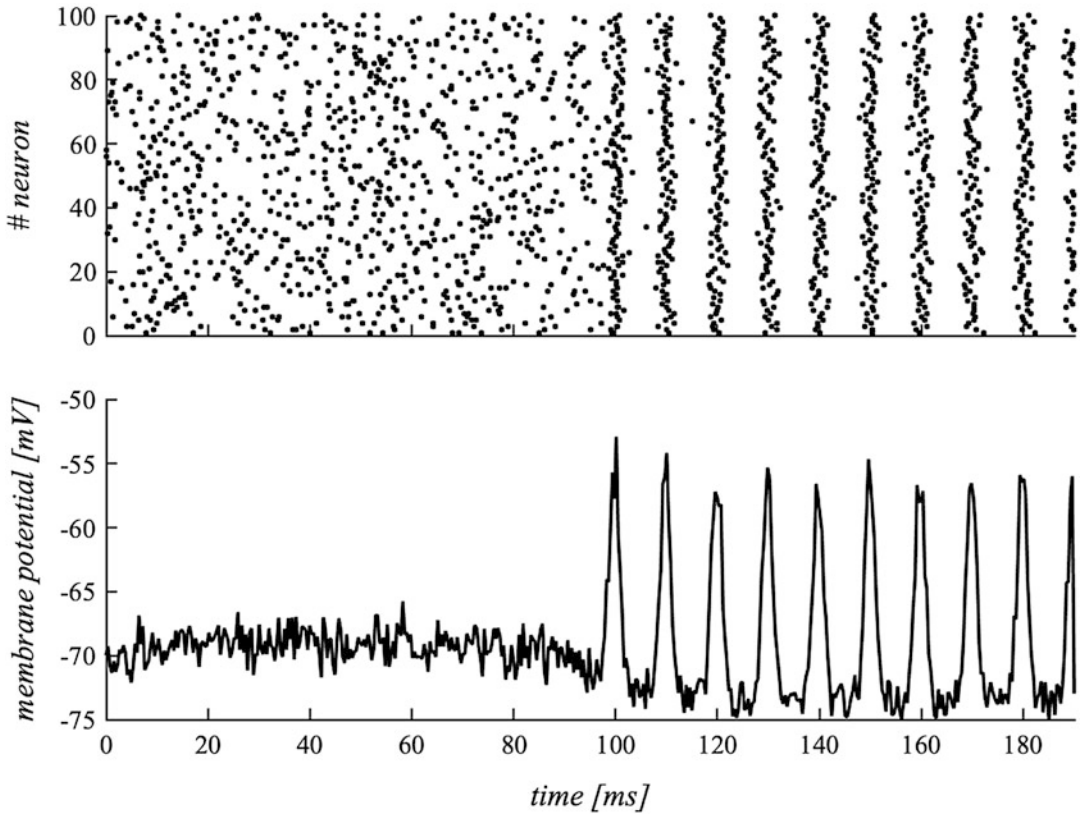

Phase Synchronization in Neural Systems, Fig. 2 Simulated spike trains of a population of 100 neurons (upper panel). At the beginning, spikes are emitted randomly causing the resulting mean-field potential (~local field potential) to weakly fluctuate around the resting potential of about −70 mV (lower panel). At around 100 ms, the neurons spontaneously synchronize their phases yielding a mean membrane potential that oscillates at about 100 Hz. The frequencies in local field potentials are usually higher than those observed in encephalographic recordings – cf. Fig. 1. To generate the figure, we used a stochastic extension of the Kuramoto model (7) and defined spike events via Poincaré sections of the phase oscillators' trajectories (Deschle et al. 2019). At around $t \approx 90$ ms, the coupling strengths κ was increased beyond the critical value κ_c, and, after a brief transient period, the population fires in synchrony at a rate given by the mean of the oscillators natural frequencies. Note that the mean membrane potential simply resembles the population density of spikes as a function of time, here adjusted to mimic standard values of action and reversal potentials (Kandel et al. 2013). The figure was inspired by Masquelier et al. (2009).

$$\text{if } v_j \text{ reaches } +\infty \text{ then neuron } j \text{ emits a spike and its membrane potential } v_j \text{ resets to } -\infty. \tag{1b}$$

In the absence of any coupling between neurons, i.e., if $J = G = 0$ holds, the neurons are either quiescent or oscillate dependent on their individual, external input $\eta_j < 0$ or $\eta_j > 0$, respectively. More realistic, however, is the case in which the neurons are coupled to one another (Pietras et al. 2019). For coupling through chemical synapses, we adopt an obvious synaptic activation function

$$S(t) = \frac{1}{N}\sum_{j=1}^{N}\frac{1}{\tau_S}\int_{t-\tau_s}^{t}\sum_{k}\delta\left(t' - t_j^k\right)dt' \tag{1c}$$

i.e., a summation of incoming spikes; t_j^k denotes the time of the k-th Dirac delta-spike of the j-th neuron and τ_S is a synaptic time constant. The synaptic strength J can be positive or negative

implying the chemical synapses are excitatory or inhibitory, respectively. For electric coupling, we assume that it is diffusively modulated by the population's mean membrane voltage

$$V = \frac{1}{N}\sum_{j=1}^{N} v_j. \tag{1d}$$

As it will turn out, electrical coupling tends to balance the membrane potentials v_j and may, hence, facilitate synchronization between neurons. Yet, if a sufficiently large portion of neurons in the population is inactive, gap junctions can suppress oscillations and desynchronize neuronal activities (Connors 2017; Alcamí and Pereda 2019).

Following Montbrió et al. (2015) and Luke et al. (2013), we consider the thermodynamic limit $N \to \infty$ and define a density function ρ such that $\rho(v|\eta, t)\, dv$ denotes the fraction of neurons with membrane potentials between v and $v + dv$ at time t and external current η. For the sake of simplicity, we consider the external currents to be distributed according to a Lorentzian $\frac{\Delta}{\pi}/\left[(\eta - \overline{\eta})^2 + \Delta^2\right]$ centered around $\overline{\eta}$ with half-width Δ.

We further assume a clear separation of time scales in that the time scale of synaptic processing is much smaller than that of the membrane potentials. In fact, in the limit $\tau_S \to 0$, the synaptic interaction (1c) reduces to $S(t) = R(t)$ with $R(t)$ being the population's mean firing rate. At first glance, assuming instantaneous synaptic responses appears a limitation to our model since synaptic time scales are often considered to be longer than those of the cell membrane. However, synaptic time constants can be as small as 1.7 ms (Häusser and Roth 1997), much in the range of typical time scales of the membrane dynamics, which renders our approximation acceptable. Introducing finite time scales, e.g., via exponential or a synapse, can be realized by using the corresponding Green's functions (Haken 2006; Byrne et al. 2017). Effectively, this will cause a synaptic delay enriching the dynamical spectrum by far; see Devalle et al. (2018) for details. Here, however, we seek to highlight the effects of electric couplings as in our model they turn out to be the major ingredient for the emergence of neural oscillations.

All things considered, we find that the mean-field dynamics of the population of electrically and chemically coupled QIF neurons evolves according to

$$\begin{aligned} \tau\dot{R} &= \frac{\Delta}{\tau\pi} + 2RV - GR, \\ \tau\dot{V} &= V^2 + \overline{\eta} - (\pi\tau R)^2 + J\tau R. \end{aligned} \tag{2}$$

The common variables R and V are the already introduced mean firing rate and mean membrane potential of the population, respectively. Together they determine the total time-dependent voltage density of the population Eq. (1), which turns out to be a Lorentzian $\tau r(t)/\{[v - V(t)]^2 + [\pi\tau R(t)]^2\}$ centered at $V(t)$ with half-width $\pi\tau R(t)$. Electrical coupling leads to a narrowing of the voltage distribution ρ by decreasing the firing rate R as in (2). That is, it balances the neurons' membrane potentials and may promote synchrony, leading to their synchronized firing activity as anticipated before, and oscillations of the population firing rate can emerge. By contrast, chemical coupling merely shifts ρ through the voltage dynamics in (2). Figure 3 briefly summarizes the corresponding bifurcation scheme, but we refer to Montbrió et al. (2015) and Pietras et al. (2019) for the in-depth analysis.

Writing about neural mass modeling must not let the neural mass model by Wilson and Cowan (1972, 1973) be unnoticed. Like the neural mass model (2), it provides a comprehensive link toward a macroscopic description of the aforementioned cell assemblies (Kilpatrick 2015). The Wilson-Cowan neural mass model represents the interdependent collective neuronal dynamics in terms of the mean firing rates of the excitatory and inhibitory parts of the population, i.e., $R \to (E, I)$. It exhibits rich dynamic behavior as well as different transitions to oscillatory dynamics (Hoppensteadt and Izhikevich 1997; Borisyuk and Kirillov 1992). This makes it also exemplary for a neural oscillator model. We will exploit some of these features when addressing coupled neural masses in the parts to come.

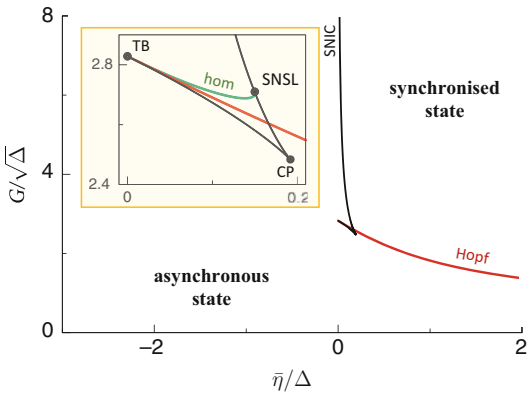

Phase Synchronization in Neural Systems, Fig. 3 Bifurcation diagram of the dynamics (2) for electrical coupling only ($J = 0$) is characterized by the presence of codimension-2 points (*TB* Takens-Bogdanov; *SNSL* saddle-node separatrix loop, Cusp) at $\bar{\eta} \geq 0$. The region of synchronization, i.e., oscillatory population activity, is limited by supercritical Hopf (red), SNIC (black), and homoclinic (green) bifurcations. Inset: Enlargement of the region near the three codimension-2 points. SN – saddle-node bifurcation; see Pietras et al. (2019) for details

We consider N_e excitatory and N_i inhibitory neurons and denote by e_n and i_n the firing rate of a single excitatory and inhibitory neuron, respectively. The respective mean firing rates can be given by the averages $E = \frac{1}{N_e}\sum_{n=1}^{N_e} e_n$ and $I = \frac{1}{N_i}\sum_{n=1}^{N_i} i_n$. Every neuron receives inputs from all other neurons within the population and every excitatory neuron receives an external input η_j, whose average is given by $\bar{\eta} = \frac{1}{N_e}\sum_{n=1}^{N_e}\eta_n$. Once the sum of all inputs exceeds a certain threshold θ_n, a neuron elicits a spike. For a particular distribution of threshold values across the population, one can assign a sigmoidal activation function $\mathcal{S}[x] = 1/(1+e^{-x})$ with population-specific threshold values by Θ_E and Θ_I for the excitatory and inhibitory part, respectively. Then, the population dynamics follows

$$\begin{aligned}\tau_E\dot{E} &= -E(t) + [1 - r_E E]\times \\ &\quad \times\mathcal{S}[a_E(c_{EE}E - c_{IE}I - \Theta_E + \bar{\eta})] \\ \tau_I\dot{I} &= -I(t) + [1 - r_I I]\times \\ &\quad \times\mathcal{S}[a_I(c_{EI}E(t) - c_{II}I - \Theta_I)],\end{aligned} \tag{3}$$

with c_{kj} with $k, j \in \{E, I\}$ indicating the strength of interaction between the different parts within the population, and a_E, a_I define the slopes of the transfer function. The expressions $[1 - r_E E]$ and $[1 - r_I I]$ represent the refractory dynamics of the excitatory and inhibitory subpopulations, respectively, that we here ignore by setting $r_E = r_I = 0$ (Pinto et al. 1996). Like model (2) also the dynamics (3) can exhibit self-sustained oscillations and multi-stability (Wilson and Cowan 1972; Hoppensteadt and Izhikevich 1997; Borisyuk and Kirillov 1992); the bifurcation diagram is depicted in Fig. 4.

Synchronization Between Neural Populations: Coupled Neural Masses

The Wilson-Cowan model may be considered a generic description of a densely connected neural population as in a particular cortical region (Breakspear 2017; Daffertshofer and van Wijk 2011). Hence we use it to build a cortical network model. For this, we connect N different populations of excitatory and inhibitory neurons in a region (E_j, I_j) via their excitatory parts (Daffertshofer and van Wijk 2011; Schuster and Wagner 1990; Daffertshofer et al. 2018) – this creates a network of $j = 1,\ldots, N$ nodes; see Fig. 5 for illustration.

In line with (3), we assume the locally averaged fire rates at every node to obey the dynamics

$$\begin{aligned}\tau_E\dot{E}_j &= E_j + \mathcal{S}\Big[a_E\Big(c_{EE}E_j - c_{IE}I_j - \Theta_E + \bar{\eta}_j + \\ &\quad + \frac{\kappa}{N}\sum_{k=1}^{N} C_{jk}\big(E_k - E_k^0\big)\Big)\Big] \\ \tau_I\dot{I}_j &= -I_j + \mathcal{S}\big[a_I\big(c_{EI}E_j - c_{II}I_j - \Theta_I\big)\big],\end{aligned} \tag{4}$$

where E_k^0 is the unstable fixed point solution of neural mass (E_k, I_k) in the absence of coupling. Importantly, $0 \leq \kappa \ll 1$ denotes the overall coupling strength, $C = \{C_{jk}\}$ is an adjacency matrix resembling structural connectivity between

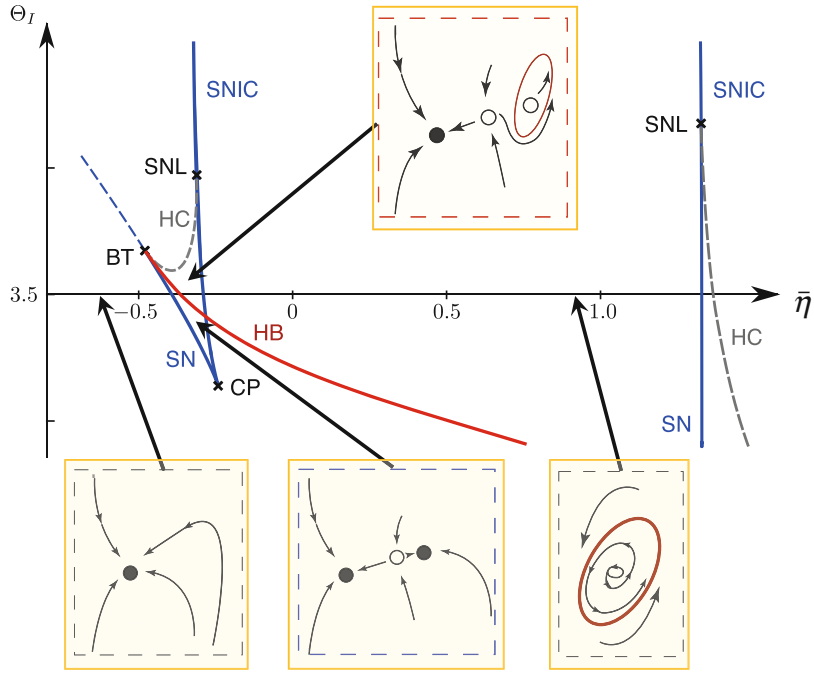

Phase Synchronization in Neural Systems, Fig. 4 Bifurcation diagram of the uncoupled Wilson-Cowan model (4). By increasing $\overline{\eta}$, one can identify four different dynamical regimes (see insets) that are separated by bifurcation boundaries; filled/empty dots, stable/unstable fixed points; red, stable limit cycle. In the lower right inset, the limit cycle is the unique attractor of the dynamics. *SN* saddle-node bifurcation, *HB* Hopf bifurcation, *HC* homoclinic bifurcation, *BT* Bogdanov-Takens point, *CP* cusp point, *SNL* saddle-node loop bifurcation, *SNIC* saddle node on invariant cycle bifurcation; see Pietras and Daffertshofer (2019) for more details

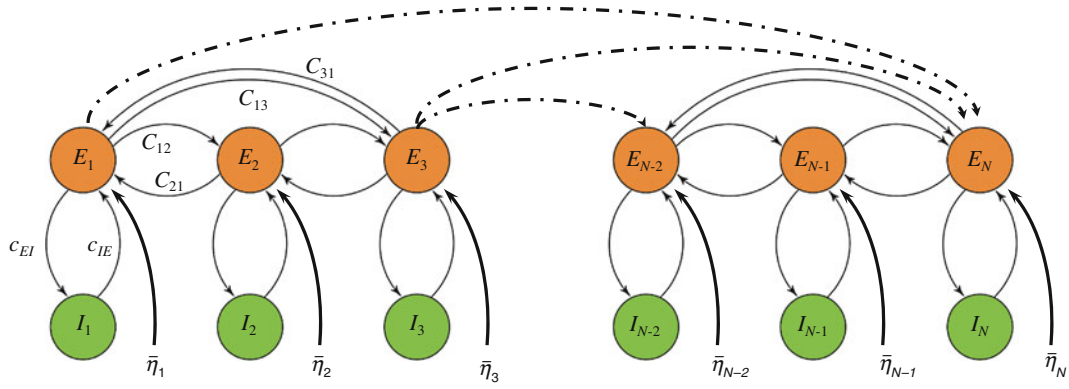

Phase Synchronization in Neural Systems, Fig. 5 Network of coupled Wilson-Cowan neural masses. Each neural population k contains excitatory and inhibitory units (E_j and I_j), which are internally coupled with strengths c_{nm}, $n, m \in \{E, I\}$. The populations receive external inputs $\overline{\eta}_j$. Interaction between two neural masses j, k occurs via their respective excitatory parts only, where C_{jk} denotes the connectivity whether node j receives input from node k.

cortical regions $(j, k) = 1,\ldots, N$, and the population specific average input *fjj* may differ across the different cortical regions.

Limit-cycle oscillations emerge in general through a bifurcation, which – and also whose type – can be revealed by looking at the

eigenspectrum of the linearized dynamics. In the case of a Hopf bifurcation, oscillatory dynamics evolve on a stable limit cycle around an unstable fixed point. We therefore expect that for an uncoupled (E_j, I_j) node, the Jacobian of the Wilson-Cowan dynamics (4) evaluated at the unstable fixed point (E_j^0, I_j^0) has a pair of complex conjugate eigenvalues with negative real part, which corresponds to the distance $\mu := \overline{\eta}_j - \overline{\eta}_H$ to the Hopf bifurcation point. One typically expresses the dynamics in terms of the deviations $\boldsymbol{x}_j = \left(E_j - E_j^0(\mu), I_j - I_j^0(\mu)\right)$ around the unstable fixed points. Approximating the sigmoidal activation function S up to third order and applying some laborious algebraic transforms (Pietras and Daffertshofer 2019), one can derive a fairly generic form of the dynamics (4) that reads

$$\dot{\boldsymbol{x}}_j = \boldsymbol{L}\boldsymbol{x}_j + \boldsymbol{T}^{-1}\boldsymbol{f}\left(\boldsymbol{T}\boldsymbol{x}_j; \mu\right) + \\ + \kappa \boldsymbol{T}^{-1} \sum_{k=1}^{N} \boldsymbol{g}\left(\boldsymbol{T}\boldsymbol{x}_j, \boldsymbol{T}\boldsymbol{x}_k\right). \tag{5}$$

Here $\boldsymbol{L}$ is the Jordan real form of the dynamics' Jacobian $\boldsymbol{J}$, $\boldsymbol{T}$ the matrix containing the eigenvectors of $\boldsymbol{J}$. The function $\boldsymbol{f}$ includes all components within node $\boldsymbol{j}$ that contribute to its dynamical change, and $\boldsymbol{g}$ covers all the between-node interaction, i.e., the last term of the right-hand side of the $\dot{E}_j$ dynamics in (4) now given as coupling between the nodes $\boldsymbol{x}_j$ and $\boldsymbol{x}_k$. The dynamics (5) exhibits qualitatively the same behavior as (4), but due to the Jordan real form, a circular symmetry of the limit cycle is imposed on the full dynamics.

In the immediate vicinity of the Hopf bifurcation point, one can exploit the separation of time scales of phase and amplitude dynamics and readily transform (5) into $\boldsymbol{x}_j = (x_j, y_j) = (R_j \cos(\theta_j), R_j \sin(\theta_j))$, where R_j and $\theta_j = \Omega t + \phi_j$ are amplitude and phase (deviations) of the oscillations at node j, which are slowly varying with respect to the (mean) frequency Ω (Haken 2004), here defined over the eigenvalues at the Hopf point, $\Omega = \omega(0)$. Near the onset of oscillations through a supercritical Hopf bifurcation, $R_j \ll 1$ is small and, thus, the right-hand side of (5) is at least of order $O(R_j)$. Given the slower time scales of R_j and $\phi_j = \theta_j - \Omega t$, one can average over one cycle $T = 2\pi/\Omega$. In line with Daffertshofer et al. (2018), this direct averaging of the dynamics (5) yields the phase model

$$\dot{\theta}_j = \omega_j + \sum_{k=1}^{N} D_{jk} \sin\left(\theta_k - \theta_j + \Delta_{jk}\right) \tag{6}$$

with coupling $D_{jk} = \frac{\kappa}{2N} a_E S'_E \Lambda_j C_{jk} \left(R_k / R_j\right)$ and finite phase lag $\Delta_{jk} = \arctan(\rho_j) - \Omega\tau_{jk}$. Here we abbreviated $\Lambda_j^2 = 1 + \rho_j^2$ with $\rho_j = \frac{\kappa}{\omega_j}\left(a_E c_{EE} S'_E + a_I c_{II} S'_I\right)$ as well as $\omega_j = a_E a_I c_{IE} c_{EI} S'_E S'_I - \frac{1}{4}\left(a_E c_{EE} S'_E + a_I c_{II} S'_I\right)^2$; and, $S'_{E/I}$ denotes the first derivative of sigmoid $\mathcal{S}$ evaluated at the fixed points E_j^0/I_j^0 of (4). We would like to note that we included some time delays τ_{jk} between nodes $\boldsymbol{x}_j$ and $\boldsymbol{x}_k$ in the coupling function $\boldsymbol{g}(\boldsymbol{x}_j, \boldsymbol{x}_k) \to g(\boldsymbol{x}_j(t), \boldsymbol{x}k(t - \tau_{kj}))$; see Pietras and Daffertshofer (2019) and Daffertshofer et al. (2018) for more details. The dynamics (6) resembles the Kuramoto-Sakaguchi model with phase lag $\left|\Delta_{jk}\right| \leq \frac{\pi}{2}$.

Importantly, a transition to full synchronization occurs if the coupling strength κ exceeds a critical value κ_c as illustrated in Fig. 6. There we used the case in which the dynamics can be rewritten as

$$\dot{\theta}_j = \omega_j + \frac{\kappa}{N} \sum_{k=1}^{N} \sin\left(\theta_k - \theta_j\right) \tag{7}$$

which, in fact, is the seminal Kuramoto model (Kuramoto 1984); see also below.

Using more general phase reduction techniques may generate phase oscillator models that contain higher harmonics (Pietras and Daffertshofer 2019). The absence of higher harmonics hampers, e.g., clustering effects. In any case, however, the network dynamics of (weakly) coupled Wilson-Cowan neural masses can be expressed in terms of a corresponding phase model

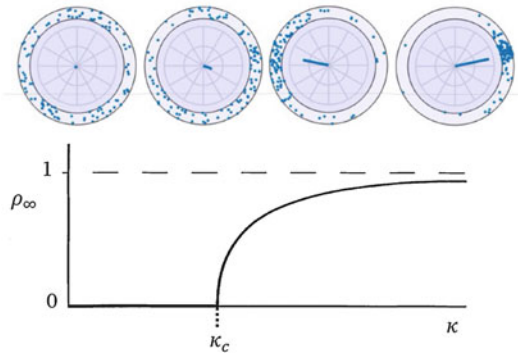

Phase Synchronization in Neural Systems, Fig. 6 Phase oscillators and phase synchronization. The distribution of phases θ_j of the neural oscillators is plotted as points $e^{i\theta_j}$ on the complex unit circle for increasing coupling strength κ. Their average over the population is the Kuramoto order parameter z, shown within the unit circle (top panels from left to right). The phase divergence $\rho = |z|$ describes the degree of synchronization and undergoes a pitchfork bifurcation from asynchrony, $\rho_\infty = 0$, to partial synchrony, $\rho_\infty > 0$, at a critical coupling strength $\kappa_c = 2\Delta$, with Δ being the half-width of the (Lorentzian) density of the oscillators' natural frequencies; see also Kuramoto (1984). Lower panel shows the asymptotic solution of (12) that reads

$$\dot{\theta}_j = \omega_j + \frac{\kappa}{N}\sum_{k=1}^{N} C_{jk} H\left(\theta_j - \theta_k\right), \qquad (8)$$

$$\rho_\infty = \rho(t \to \infty) = \left\{ 0 \text{ for } \kappa < 2\Delta, \sqrt{1 - \frac{2\Delta}{\kappa}} \text{otherwise} \right\}.$$

where the phase interaction function $H(\psi)$ admits a "simple" representation as a Fourier series

$$H(\psi) = \sum_{n \geq 0} \alpha_n \cos(n\psi) + \beta_n \sin(n\psi). \qquad (9)$$

With such an expression at hand, one can seek to estimate the Fourier amplitudes α_n, β_n that readily provide crucial information about global synchronization of the full neural network or whether clustering of only a subset of network nodes occurs; see Pietras and Daffertshofer (2019) for more details.

Predicting Effects of Phase Synchronization

Mathematical theory and computational modeling go hand in hand with experimental neuroscientific research. Modeling helps to unravel the mechanisms underlying complex behavior. Not only can it provide proper and robust quantitative descriptions, but it also helps to formulate hypotheses and predict future outcome of experimental research. Many physiologically motivated neuronal models have been put forward to investigate synchronization properties in neural systems. Given their inherent complexity, a thorough analysis can be challenging even despite ever-increasing computational capacities. In some cases, the dynamics of neural systems can be simplified to *coupled phase oscillators models*, which often takes on a modified form of a network of seminal Kuramoto oscillators (7) (Daffertshofer and van Wijk 2011; Schuster and Wagner 1990; Rodrigues et al. 2016; Breakspear et al. 2010; Ton et al. 2014; Cabral et al. 2014; Tasseff et al. 2014; Sadilek and Thurner 2015; Schmidt et al. 2015). For the Kuramoto model, there exists a rigorous theory to describe the state of the network with very few macroscopic variables. Following either the Watanabe-Strogatz (Watanabe and Strogatz 1994) or the Ott-Antonsen theory (Ott and Antonsen 2008), the time evolution of these macroscopic variables can be derived exactly under some quite generic conditions. It thus becomes possible to study low-dimensional behavior of the collective dynamics in a straightforward way.

We use the Kuramoto model to illustrate this. In brief, given the model (7) of a population of phase oscillators θ_j with $j = 1,\ldots, N$, one introduces the Kuramoto *order parameter* (Kuramoto 1984)

$$z = \frac{1}{N}\sum_{j=1}^{N} e^{i\theta_j} \qquad (10)$$

to describe the population's common dynamics. This order parameter can be expressed via the population density $p(\theta, t; \omega)$. The density contains both frequencies and phases $p(\theta, t; \omega) = q(\omega) f(\theta,$

$t; \omega$), where the phase density, in general, has the Fourier series $f(\theta, t; \omega) = \frac{1}{2\pi}\sum_{n=-\infty}^{\infty} f_n(t; \omega)e^{in\theta}$. Substituting this into (7) motivates the ansatz $f_n = \alpha^{|n|}$ with $\alpha = f_1 = z^*$. Considering a Lorentzian frequency density $q(\omega) = \frac{\Delta}{\pi}/\left[(\omega - \omega_0)^2 + \Delta^2\right]$, the exact solution of (7) for $N \to \infty$ yields the *order parameter dynamics*

$$\dot{z} = \left(i\omega_0 - \Delta + \frac{\kappa}{2}\right)z - \frac{\kappa}{2}|z|^2 z. \qquad (11)$$

Accordingly, the *phase divergence* $\rho = |z|$ follows the well-established equation of motion

$$\dot{\rho} = -\left(\Delta - \frac{\kappa}{2}\right)\rho - \frac{\kappa}{2}\rho^3 \qquad (12)$$

while the mean phase $\psi = \sphericalangle(z)$ follows $\dot{\psi} = \omega_0$. The explicit solution of (12) can be given by

$$\rho(t)\sqrt{\frac{\Delta - \frac{\kappa}{2}}{\left(\Delta - \frac{\kappa}{2}\left(1 - \rho_0^2\right)\right)e^{(2\Delta-\kappa)t} - \frac{\kappa}{2}\rho_0^2}\rho_0} \qquad (13)$$

quantifying (one minus) the width of the density of phases

$$f(\theta, t; \omega) = \frac{1 - \rho^2}{1 - 2\rho\cos\theta + \rho^2}. \qquad (14)$$

Hence, for some initial condition ρ_0, the dynamics' relaxation time becomes

$$\tau = \frac{1}{2\Delta - \kappa}\ln\left[\frac{2\Delta + \kappa\left(\rho_\tau^2 - 1\right)}{2\Delta + \kappa\left(\rho_0^2 - 1\right)} \cdot \frac{\rho_0^2}{\rho_\tau^2}\right] \qquad (15)$$

with $\rho(\tau) = \rho_\tau$. The value ρ_τ can be determined using the asymptotic solution as we set $\rho_\tau = \rho_0 - \gamma(\rho_0 - \rho_\infty)$ with, e.g., $\gamma = 99.9\%$.

Many studies speculated about the relevance of the (finite) time it takes for a population of neural oscillators to approach synchrony or to desynchronize, often in the context of the binding problem outlined in the introductory paragraph. Already by looking at Fig. 2, it becomes apparent that the local field potential of a group of neurons can only be of significant value if their phase density is sufficiently narrow. At larger scale, classic experimental paradigms for investigating relaxation times of phase synchronization involve event- or moton-related responses as sketched in Fig. 7.

Final Notes

Phase oscillator models help to explain how changes in the local dynamics affect functional connectivity, how neural synchronization can be achieved, and how functional clusters or modules are generated through remote synchronization. These models have also been used to investigate the interplay between structure (anatomy) and function, including effects of cortical lesions on the overall brain dynamics (Honey and Sporns 2008; Vása et al. 2015). Given their mathematical ease, they are particularly suited to explore the emergence of (de-)synchronized states per se and the corresponding relationship between them, but also to tackle even more generic characteristics such as self-organized criticality.

The use of phase oscillator models, however, is not without a risk: the reduction of a (network) dynamics to a phase oscillator model requires great care (Pietras and Daffertshofer 2019). Any (heuristic) approximation of an oscillatory neural network via a network of phase oscillators has to withstand comparison with the "original" dynamics and starting-off with "just" the phase oscillator network may lose contact with biophysical or physiological reality.

Summary

Rhythmic behavior of a neural population implies an oscillatory dynamics of one or more macroscopic variables. The corresponding phase space exhibits a limit cycle that, if stable, attracts the population dynamics. If this attraction is

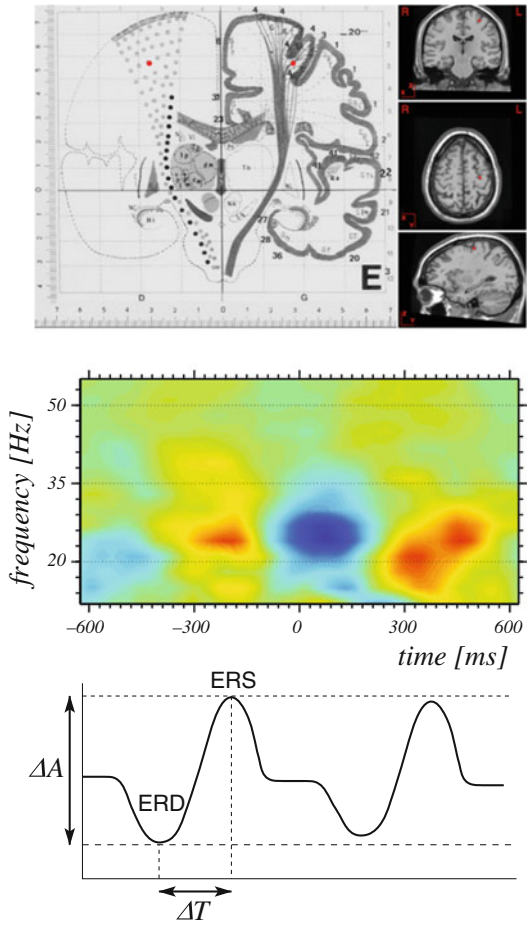

Phase Synchronization in Neural Systems, Fig. 7 Rhythmic motor performance is accompanied by a rhythmic modulation of beta-range oscillatory activity in primary motor cortices; cf. Fig. 1. The middle panel displays the time-dependent changes of the spectral power of a movement cycle as assessed via MEG (Houweling et al. 2010). The beta activity displays event-related synchronization and de-synchronization (ERS and ERD, i.e., red and blue patches, respectively). If the movement cycle is too short, ERS and ERD cannot develop due to the finite relaxation time of the underlying phase dynamics, and motor performance can no longer be timed.

sufficiently fast, the dynamics away from the limit cycle can be approximated by the dynamics on the limit cycle. We illustrated this for the case of a single population. In such a case, the high-dimensional dynamics of neuronal oscillators can be uniquely identified by a one-dimensional phase variable. The phase reduction becomes especially useful when studying a network of interacting neural oscillators as we showed for the case of coupled Wilson-Cowan neural mass models. The resulting phase models can, in general, be analyzed along well-established techniques for networks of coupled phase oscillators. The resulting findings on synchronization properties can mimic oscillatory activity in neural masses as observed in experiments. They also help understanding effects of changes in synchronization for the macroscopic functioning of the nervous system.

Acknowledgments We would like to thank Federico Devalle, Ernest Montbrió, and Alex Roxin for the many discussions about interacting QIF neurons. Peter Beek, Sanne Houweling, Peter Praamstra, and Bernadette van Wijk provided the material that here served to illustrate some recent experimental findings on the phase dynamics in the human motor system. This work received financial support via ITN COSMOS funded by the EU Horizon 2020 research and innovation program under the Marie Skłodowska-Curie Grant Agreement No. 642563.

Bibliography

Alcamí P, Pereda AE (2019) Beyond plasticity: The dynamic impact of electrical synapses on neural circuits. Nat Rev Neurosci 20(5):253–271

Amari SI (1977) Dynamics of pattern formation in lateral-inhibition type neural fields. Biol Cybern 27(2):77–87

Borisyuk RM, Kirillov AB (1992) Bifurcation analysis of a neural network model. Biol Cybern 66(4):319–325

Breakspear M (2017) Dynamic models of large-scale brain activity. Nat Neurosci 20(3):340–352

Breakspear M, Heitmann S, Daffertshofer A (2010) Generative models of cortical oscillations: Neurobiological implications of the Kuramoto model. Front Hum Neurosci 4:190

Brunel N, Hakim V (1999) Fast global oscillations in networks of integrate-and-fire neurons with low firing rates. Neural Comput 11(7):1621–1671

Buzsaki G (2006) Rhythms of the brain. Oxford University Press

Byrne Á, Brookes MJ, Coombes S (2017) A mean field model for movement induced changes in the beta rhythm. J Comput Neurosci 43(2):143–158

Cabral J, Kringelbach ML, Deco G (2014) Exploring the network dynamics underlying brain activity during rest. Prog Neurobiol 114(Supplement C):102–131

Connors BW (2017) Synchrony and so much more: Diverse roles for electrical synapses in neural circuits. Dev Neurobiol 77(5):610–624

Coombes S (2010) Large-scale neural dynamics: Simple and complex. NeuroImage 52(3):731–739

Daffertshofer A, van Wijk B (2011) On the influence of amplitude on the connectivity between phases. Front Neuroinform 5:6

Daffertshofer A, Ton R, Pietras B, Kringelbach ML, Deco G (2018) Scale-freeness or partial synchronization in neural mass phase oscillator networks: Pick one of two? NeuroImage 180:428–441

Dauwels J, Vialatte F, Musha T, Cichocki A (2010) A comparative study of synchrony measures for the early diagnosis of Alzheimer's disease based on EEG. NeuroImage 49(1):668–693

Deco G, Jirsa VK, Robinson PA, Breakspear M, Friston K (2008) The dynamic brain: From spiking neurons to neural masses and cortical fields. PLoS Comput Biol 4(8):e1000092

Deschle N, Daffertshofer A, Battaglia D, Martens EA (2019) Directed flow of information in chimera states. Front Appl Math Stat 5:28

Devalle F, Montbrió E, Pazó D (2018) Dynamics of a large system of spiking neurons with synaptic delay. Phys Rev E 98(4):042214

Freeman WJ (1975) Mass action in the nervous system. Academic Press, New York

Golomb D (2007) Neuronal synchrony measures. Scholarpedia 2(1):1347

Gray CM (1994) Synchronous oscillations in neuronal systems: Mechanisms and functions. J Comput Neurosci 1(1–2):11–38

Haken H (2004) Synergetics: introduction and advanced topics. Springer, Berlin

Haken H (2006) Brain dynamics: synchronization and activity patterns in pulse-coupled neural nets with delays and noise. Springer, Berlin

Häusser M, Roth A (1997) Estimating the time course of the excitatory synaptic conductance in neocortical pyramidal cells using a novel voltage jump method. J Neurosci 17(20):7606–7625

Honey CJ, Sporns O (2008) Dynamical consequences of lesions in cortical networks. Hum Brain Mapp 29(7):802–809

Hoppensteadt FC, Izhikevich EM (1997) Weakly connected neural networks. Springer, New York

Houweling S, Beek PJ, Daffertshofer A (2010) Spectral changes of interhemispheric crosstalk during movement instabilities. Cereb Cortex 20(11):2605–2613

Hutt A, Buhry L (2014) Study of GABAergic extra-synaptic tonic inhibition in single neurons and neural populations by traversing neural scales: application to propofol-induced anaesthesia. J Comput Neurosci 37(3):417–437

Jansen BH, Rit VG (1995) Electroencephalogram and visual evoked potential generation in a mathematical model of coupled cortical columns. Biol Cybern 73(4):357–366

Jean-Philippe L, Eugenio R, Jacques M, Varela FJ (1999) Measuring phase synchrony in brain signals. Hum Brain Mapp 8(4):194–208

Kandel ER, Schwartz JH, Jessell TM et al (2013) Principles of neural science, vol 5. McGraw-Hill, New York

Kilpatrick ZP (2015) Wilson-Cowan Model. In Encyclopedia of computational neuroscience, ed. by D. Jaeger, R. Jung (Springer, New York, 2015), pp. 3159–3163

Kuramoto Y (1984) Chemical oscillations, turbulence and waves. Springer, Berlin

Lopes da Silva F, Hoeks A, Smits H, Zetterberg L (1974) Model of brain rhythmic activity. Biol Cybern 15(1):27–37

Luke TB, Barreto E, So P (2013) Complete classification of the macroscopic behavior of a heterogeneous network of theta neurons. Neural Comput 25(12):3207–3234

MacKay WA (1997) Synchronized neuronal oscillations and their role in motor processes. Trends Cogn Sci 1(5):176–183

Masquelier T, Hugues E, Deco G, Thorpe SJ (2009) Oscillations, phase-of-firing coding, and spike timing-dependent plasticity: An efficient learning scheme. J Neurosci 29(43):13484–13493

Montbrió E, Pazó D, Roxin A (2015) Macroscopic description for networks of spiking neurons. Phys Rev X 5(2):021028

Nunez PL (2000) Toward a quantitative description of large-scale neocortical dynamic function and EEG. Behav Brain Sci 23(3):371–398

Ott E, Antonsen TM (2008) Low dimensional behavior of large systems of globally coupled oscillators. Chaos 18(3):037113

Pazó D, Montbrió E (2016) From quasiperiodic partial synchronization to collective chaos in populations of inhibitory neurons with delay. Phys Rev Lett 116:238101

Pietras B, Daffertshofer A (2019) Network dynamics of coupled oscillators and phase reduction techniques. Phys Rep 819:1–105

Pietras B, Devalle F, Roxin A, Daffertshofer A, Montbrió E (2019) Exact firing rate model reveals the differential effects of chemical versus electrical synapses in spiking networks. Phys Rev E 100:042412

Pinto DJ, Brumberg JC, Simons DJ, Ermentrout GB, Traub R (1996) A quantitative population model of whisker barrels: re-examining the Wilson-Cowan equations. J Comput Neurosci 3(3):247–264

Renart A, de la Rocha J, Bartho P, Hollender L, Parga N, Reyes A, Harris KD (2010) The asynchronous state in cortical circuits. Science 327(5965):587–590

Rodrigues FA, Peron TKD, Ji P, Kurths J (2016) The Kuramoto model in complex networks. Phys Rep 610:1–98

Sadilek M, Thurner S (2015) Physiologically motivated multiplex Kuramoto model describes phase diagram of cortical activity. Sci Rep 5:10015

Sauseng P, Klimesch W (2008) What does phase information of oscillatory brain activity tell us about cognitive processes? Neurosci Biobehav Rev 32(5):1001–1013

Schmidt R, LaFleur KJR, de Reus MA, van den Berg LH, van den Heuvel MP (2015) Kuramoto model simulation of neural hubs and dynamic synchrony in the human cerebral connectome. BMC Neurosci 16(1):54

Schnitzler A, Gross J (2005) Normal and pathological oscillatory communication in the brain. Nat Rev Neurosci 6(4):285–296

Schuster H, Wagner P (1990) A model for neuronal oscillations in the visual cortex. Biol Cybern 64(1):77–82

Siettos C, Starke J (2016) Multiscale modeling of brain dynamics: From single neurons and networks to mathematical tools. Wiley interdisciplinary reviews: Biol Med 8(5):438–458

Singer W (1993) Synchronization of cortical activity and its putative role in information processing and learning. Annu Rev Physiol 55:349–374

Singer W (2007) Binding by synchrony. Scholarpedia 2(12):1657

Tasseff R, Bheda-Malge A, DiColandrea T, Bascom CC, Isfort RJ, Gelinas R (2014) Mouse hair cycle expression dynamics modeled as coupled mesenchymal and epithelial oscillators. PLoS Comput Biol 10(11):1–21

Thut G, Miniussi C, Gross J (2012) The functional importance of rhythmic activity in the brain. Curr Biol 22(16):R658–R663

Ton R, Deco G, Daffertshofer A (2014) Structure-function discrepancy: Inhomogeneity and delays in synchronized neural networks. PLoS Comput Biol 10(7): e1003736

Uhlhaas PJ, Singer W (2006) Neural synchrony in brain disorders: Relevance for cognitive dysfunctions and pathophysiology. Neuron 52(1):155–168

Van Wijk B, Daffertshofer A, Roach N, Praamstra P (2008) A role of beta oscillatory synchrony in biasing response competition? Cereb Cortex 19(6):1294–1302

Varela F, Lachaux JP, Rodriguez E, Martinerie J (2001) The brainweb: Phase synchronization and large-scale integration. Nat Rev Neurosci 2(4):229–239

Vása F, Shanahan M, Hellyer PJ, Scott G, Cabral J, Leech R (2015) Effects of lesions on synchrony and metastability in cortical networks. NeuroImage 118-(Supplement C):456–467

Wang XJ (2010) Neurophysiological and computational principles of cortical rhythms in cognition. Physiol Rev 90(3):1195–1268

Watanabe S, Strogatz SH (1994) Constants of motion for superconducting Josephson arrays. Physica 74D (3):197–253

Wilson HR, Cowan JD (1972) Excitatory and inhibitory interactions in localized populations of model neurons. Biophys J 12(1):1–24

Wilson HR, Cowan JD (1973) A mathematical theory of the functional dynamics of cortical and thalamic nervous tissue. Kybernetika 13(2):55–80

Womelsdorf T, Valiante TA, Sahin NT, Miller KJ, Tiesinga P (2014) Dynamic circuit motifs underlying rhythmic gain control, gating and integration. Nat Neurosci 17(8):1031